



Synthesis, structure and properties of new layered oxyselenides $\text{Nd}_2(\text{Fe}_{1-x}\text{Mn}_x)_2\text{Se}_2\text{O}_3$



Y. Liu^a, S.B. Zhang^{a,*}, W.J. Lu^a, L.J. Li^a, S.G. Tan^a, B. Yuan^a, J. Chen^a, Y.P. Sun^{a,b,c,*}

^a Key Laboratory of Materials Physics, Institute of Solid State Physics, Chinese Academy of Sciences, Hefei 230031, People's Republic of China

^b High Magnetic Field Laboratory, Chinese Academy of Sciences, Hefei 230031, People's Republic of China

^c University of Science and Technology of China, Hefei 230026, People's Republic of China

ARTICLE INFO

Article history:

Received 18 February 2014

Received in revised form 2 July 2014

Accepted 15 August 2014

Available online 2 September 2014

Keywords:

Solid state reaction

Crystal structure

Semiconductor

Antiferromagnetic

Thermoelectric

ABSTRACT

A new series of layered oxyselenides $\text{Nd}_2(\text{Fe}_{1-x}\text{Mn}_x)_2\text{Se}_2\text{O}_3$ ($0 \leq x \leq 0.5$) was synthesized via solid state reaction method. Their structure and properties were investigated by the X-ray powder diffraction, magnetic bulk, electrical and thermal transport measurements along with specific heat experiments. The compounds crystallize in the layered tetragonal structure with $I4/mmm$ space group and show semiconducting behavior. The large discrepancy between activation energy for conductivity, E_p (0.153–0.177 eV), and thermopower, E_S (7.0–14.8 meV), indicates the polaronic transport mechanism. Heat capacity and bulk magnetization indicate an increased ferromagnetic component of the long-range magnetic order and possible increased degree of frustration. Atomic disorder on Fe/Mn sites suppresses the temperature of the long-range order whereas intermediate alloys show a rich magnetic phase diagram.

© 2014 Elsevier B.V. All rights reserved.

1. Introduction

Layered transition-metal compounds have been extensively studied for decades owing to their novel physical properties, especially colossal magnetoresistance in layered manganites and high T_c superconductivity in cuprates. Recently, superconductivity with $T_c = 26$ K was discovered in F-doped LaOFeAs, and soon expanded to other R-based $\text{RO}_{1-x}\text{F}_x\text{FeAs}$ (R = Ce, Pr, Nd, Sm, Gd, Tb, and Dy) [1–7]. The FeAs layer is considered as basic structural unit for the superconductivity, which is similar to the CuO_2 layer in cuprates. Considering the relationship between structure and physical properties, it encourages people to search for new layered transition-metal materials.

Transition-metal oxyphnictides (oxychalcogenides) often crystallize in a two-dimensional (2D) structure due to large size difference of the oxide and pnictide (chalcogenide) ions. For instance, a series of $\text{ATi}_2\text{Pn}_2\text{O}$ (A = Na₂, Ba, (SrF)₂, (SmO)₂; Pn = As, Sb) is built with alternating A layer and anti- CuO_2 type Ti_2O layer [8–12]. The behavior of $\text{Na}_2\text{Ti}_2\text{Pn}_2\text{O}$ is similar to that of ROFeAs and AFe_2As_2 with a spin density wave (SDW) instability [9]. $\text{BaTi}_2\text{Sb}_2\text{O}$ shows superconductivity at $T_c = 1.2$ K as well as a charge density wave (CDW) or SDW transition at $T = 50$ K, and the T_c can be enhanced

via substituting Ba by Na or Bi doping in Sb sites [11,13,14]. Additionally, a family of ACuS (A = LaO, SrF, and BaF) crystallizes in layered structure with basic CuS planes [15–17]. The isovalent-substituted $\text{LaOCuS}_{1-x}\text{Se}_x$, along with the hole-doping attempts, including $\text{Ba}_{1-x}\text{K}_x\text{FCuS}$, $\text{Sr}_{1-x}\text{Na}_x\text{FCuS}$ and $\text{SrF}_{1-x}\text{O}_x\text{CuS}$, generates several transparent conductors [18–20]. More recently, the $\text{R}_2\text{T}_2\text{Q}_2\text{O}_3$ (R-2223) (R = La–Sm, T = Mn, Fe, Co and Q = S, Se) system has gathered much attention [21–28], due to its basic anti- CuO_2 -type T_2O plane and antiferromagnetic (AFM) ground state. Theoretical calculation and neutron diffraction experiments indicate an unusual frustrated AFM checkerboard spin–lattice, which hosts rich magnetic ground states and could be relevant to physics of colossal magnetoresistance in manganites and high T_c superconductivity in iron-oxyphnictides and cuprates.

Within the T_2OQ_2 layer in R-2223 system, there are three principal competing interactions: the nearest neighbor (NN) J_3 interaction of the T–T, the next nearest neighbor (NNN) J_2 interaction of nearly 90° T–Q–T, and the NNN J_1 interaction of 180° T–O–T. The parent $\text{La}_2\text{Fe}_2\text{Se}_2\text{O}_3$ adopts magnetic structure similar to that of $\text{Fe}_{1.086}\text{Te}$, with the majority spin direction in the ab plane [24,29,30]. On the other hand, $\text{La}_2\text{Mn}_2\text{Se}_2\text{O}_3$ has a G-type AFM structure with the ordered moment along the c -axis direction, where NN Mn^{2+} have opposite spin with dominant AFM $J_3 < 0$ and fully frustrated $|J_1| < J_2$ with $J_1 < 0$ and $J_2 > 0$ [24,31]. The evolution of structure and magnetic properties tuned by Fe/Mn ratio in $\text{La}_2(\text{Fe}_{1-x}\text{Mn}_x)_2\text{Se}_2\text{O}_3$ was subsequently investigated [27], and

* Corresponding authors. Address: Key Laboratory of Materials Physics, Institute of Solid State Physics, Chinese Academy of Sciences, Hefei 230031, People's Republic of China (Y.P. Sun).

E-mail addresses: sbzhang@issp.ac.cn (S.B. Zhang), ypsun@issp.ac.cn (Y.P. Sun).

show a rich magnetic phase diagram. In the series of $\text{La}_2(\text{Fe}_{1-x}\text{Mn}_x)_2\text{Se}_2\text{O}_3$, long-range magnetic order competes with disorder induced by geometric spin frustration. Atomic disorder on Fe/Mn sites tips this balance and promotes the frustration. However, no other doping attempt is seen so far, probably due to the limit of lattice match between R_2O_2 and T_2OSe_2 layers. Free et al. summarized that the Fe_2OSe_2 layer shows an optimum size match with R_2O_2 for the widest range of $R = \text{La}–\text{Sm}$, whereas the Mn_2OSe_2 layer reduces to it with $R = \text{La}–\text{Pr}$ [24].

In this paper, we successfully synthesized a new series of $\text{Nd}_2(\text{Fe}_{1-x}\text{Mn}_x)_2\text{Se}_2\text{O}_3$ ($0 \leq x \leq 0.5$) by solid state reaction, and investigated the structure and physical properties via a wide range of techniques, including the X-ray diffraction (XRD), magnetic bulk, electrical and thermal transport measurements along with specific heat experiments.

2. Experimental

$\text{Nd}_2(\text{Fe}_{1-x}\text{Mn}_x)_2\text{Se}_2\text{O}_3$ ($0 \leq x \leq 0.5$) polycrystals were synthesized via solid state reaction using Nd_2O_3 (99.99%), Mn (99.9%), Fe (99.9%) and Se (99.95%) powder as starting materials. Nd_2O_3 was dried by heating in air at 1173 K for 20 h before using. The raw materials were weighed according to the stoichiometric ratio, thoroughly grounded, pressed into pellets and then sealed in evacuated quartz tubes (10^{-3} Pa). The tubes were heated to 1273 K and reacted for 24 h followed by furnace cooling. This process was repeated several times to ensure homogeneity.

The powder XRD was performed using a Philips X'Pert PRO X-ray diffractometer with $\text{Cu K}\alpha$ radiation ($\lambda = 1.54 \text{ \AA}$). The structural parameters were obtained by using the Rietveld method with the X'Pert Plus software. The average stoichiometry was determined by examination of multiple points using X-ray energy dispersive spectroscopy (EDS) with a scanning electron microscopy (SEM). The EDS results indicate that the actual concentration x is close to the nominal one. Thermal, transport, and magnetic measurements were carried out in a Quantum Design PPMS-9 and MPMS-5.

3. Results and discussion

3.1. Structure

Fig. 1(a) shows the powder XRD patterns for $\text{Nd}_2(\text{Fe}_{1-x}\text{Mn}_x)_2\text{Se}_2\text{O}_3$ ($0 \leq x \leq 0.5$), scanning over a 2θ range of $15–90^\circ$ at room

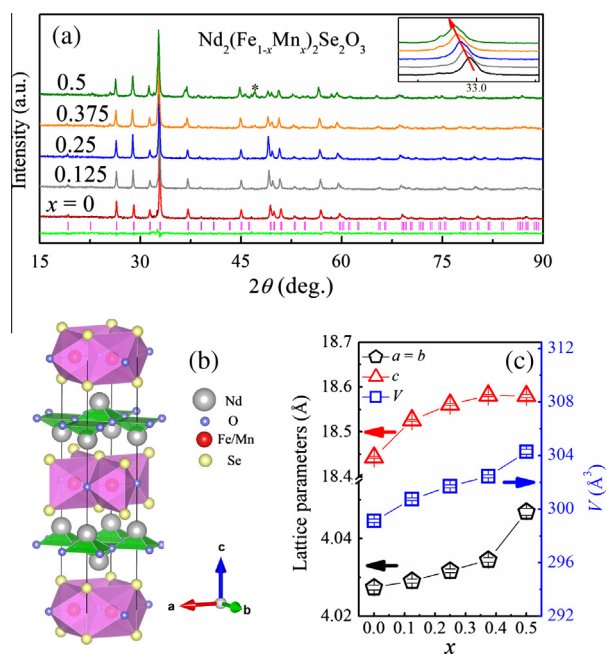


Fig. 1. (a) The powder XRD patterns for $\text{Nd}_2(\text{Fe}_{1-x}\text{Mn}_x)_2\text{Se}_2\text{O}_3$ ($0 \leq x \leq 0.5$) at $T = 300 \text{ K}$. (b) Crystal structure. (c) The evolution of lattice parameters ($a = b$, c) and unit cell volume (V).

temperature. The reflections can be well indexed with a tetragonal unit cell. The diffraction index (hkl) obeys $h + k + l = \text{even numbers}$, suggesting a body-centered lattice. For clarify, we depicted the refinement result for $\text{Nd}_2\text{Fe}_2\text{Se}_2\text{O}_3$ ($x = 0$) using the space group $I4/mmm$. With increasing x , the diffraction peak gradually shifts to lower angle degree, suggesting an expansion of the lattice. The enlargement of the (112) peak is shown in the inset of Fig. 1(a). It can be explained by the increase of the ionic sizes, $r_{\text{Mn}^{2+}}$ (0.80 \AA) $>$ $r_{\text{Fe}^{2+}}$ (0.74 \AA). However, we notice that a tiny impurity peak emerges as $x = 0.5$, marked by an asterisk, reflecting a limit solid solubility. Fig. 1(b) shows the crystal structure of $\text{Nd}_2(\text{Fe}_{1-x}\text{Mn}_x)_2\text{Se}_2\text{O}_3$, which is built up by stacking Nd_2O_2 and $(\text{Fe}/\text{Mn})_2\text{OSe}_2$ layers alternatively along c axis. The substitution with larger Mn^{2+} ions leads to an expansion of the $(\text{Fe}/\text{Mn})_2\text{OSe}_2$ slabs, and brings the final mismatch between the Nd_2O_2 layer and $(\text{Fe}/\text{Mn})_2\text{OSe}_2$ slabs with $x > 0.5$. The evolution of the lattice parameters ($a = b$, c) and the unit cell volume (V) are shown in Fig. 1(c). The values of $\text{Nd}_2\text{Fe}_2\text{Se}_2\text{O}_3$ ($x = 0$) ($a = 4.0270(6) \text{ \AA}$ and $c = 18.443(2) \text{ \AA}$) gradually increase to those of $\text{Nd}_2\text{FeMnSe}_2\text{O}_3$ ($x = 0.5$) ($a = 4.0445(9) \text{ \AA}$ and $c = 18.576(4) \text{ \AA}$). The unit cell volume (V) expansion ($= (V_{x=0.5} - V_{x=0})/V_{x=0}$) is about 1.6% and shows approximately linear dependence, indicating the well substitution in Fe/Mn sites. The structural details are summarized in Table 1, obtained by the Rietveld method with the X'Pert Plus software.

Fig. 2(a) depicts the $(\text{Fe}/\text{Mn})_2\text{OSe}_2$ plane from a vertical view with Se atoms puckering above and below the square $(\text{Fe}/\text{Mn})_2\text{O}$ flat. The evolution of the nearest intralayer Fe/Mn–Fe/Mn distance ($d_{\text{Fe}/\text{Mn}-\text{Fe}/\text{Mn}}$), together with the Fe/Mn–O and Fe/Mn–Se bond distances ($d_{\text{Fe}/\text{Mn}-\text{O}}$ and $d_{\text{Fe}/\text{Mn}-\text{Se}}$), is shown in Fig. 2(b). For $\text{Nd}_2\text{Fe}_2\text{Se}_2\text{O}_3$ ($x = 0$), we calculated the valence of Fe ions using the bond valence sum (BVS) formula in which each bond with a distance d_{ij} contribute a valence $v_{ij} = \exp[(R_{ij} - d_{ij})/0.37]$ with R_{ij} as an empirical parameter and the total valences of atom i , V_i equals $V_i = \sum_j v_{ij}$ [32,33]. The calculated valence of Fe ions is +2.02, confirming the existence of Fe^{2+} ionic state. In addition, the nearest intralayer Fe–Fe distance of $\text{Nd}_2\text{Fe}_2\text{Se}_2\text{O}_3$ ($x = 0$) is $d_{\text{intra}} = 2.8475(3) \text{ \AA}$ while the nearest interlayer Fe–Fe distance is $d_{\text{inter}} = 9.2215(10) \text{ \AA}$. The ratio of $d_{\text{inter}}/d_{\text{intra}}$ is about 3.24, indicating small interlayer spin correlations. All the distances increase with x due to larger Mn^{2+} radius, as shown in Fig. 2(b). However, the ratio of $d_{\text{Fe}/\text{Mn}-\text{Fe}/\text{Mn}}:d_{\text{Fe}/\text{Mn}-\text{Se}}$ gradually decrease from 1.041(2) for $x = 0$ to 1.030(3) for $x = 0.5$. Fig. 2(c) shows the distorted octahedral environment of each $\text{Fe}^{2+}/\text{Mn}^{2+}$ ion, with two axial O^{2-} ions and four equatorial Se^{2-} ions. The evolution of the bond angles of $\alpha_{\text{Se}-\text{Fe}/\text{Mn}-\text{Se}}$ is depicted in Fig. 2(d).

3.2. Transport properties

The temperature-dependent electrical resistivity (ρ) for $\text{Nd}_2(\text{Fe}_{1-x}\text{Mn}_x)_2\text{Se}_2\text{O}_3$ ($0 \leq x \leq 0.5$) is shown in Fig. 3, which displays an obviously semiconducting behavior. The $\rho(T)$ of $\text{Nd}_2\text{Fe}_2\text{Se}_2\text{O}_3$ is smaller than it of $\text{La}_2\text{Fe}_2\text{Se}_2\text{O}_3$ at room temperature. However, the Mn-substitution is adverse to further improve its electrical conductivity in $\text{Nd}_2(\text{Fe}_{1-x}\text{Mn}_x)_2\text{Se}_2\text{O}_3$. The 3d electrons of $\text{Fe}^{2+}/\text{Mn}^{2+}$, though being partially filled, are practically localized. The studies of $\text{A}_2\text{F}_2\text{Fe}_2\text{OQ}_2$ ($A = \text{Sr, Ba}$; $Q = \text{S, Se}$) indicate that they are Mott insulators with narrowing 3d electronic bands due to strong correlation effects [34]. The series of $\text{Nd}_2(\text{Fe}_{1-x}\text{Mn}_x)_2\text{Se}_2\text{O}_3$ ($0 \leq x \leq 0.5$) could also be regarded as correlation-induced magnetic semiconductors or Mott insulators, and therefore, it is not strange with the viewpoint of electron hopping between adjacent unpaired spins in the $\text{Fe}^{2+}/\text{Mn}^{2+}$ sites. The distance of the nearest Fe/Mn–Fe/Mn becomes larger with increasing x , which is more difficult for electron hopping. In generally, there are three models probably well fitting the observed $\rho(T)$ curve. (1) The thermally activated model: $\rho(T) = \rho_0 \exp(E/k_B T)$, where ρ_0 is the prefactor, E

Download English Version:

<https://daneshyari.com/en/article/1610358>

Download Persian Version:

<https://daneshyari.com/article/1610358>

[Daneshyari.com](https://daneshyari.com)